Simulating the built environment for another globally distributed species

Derek Morville Mitchell[1]
University of Leeds, Leeds, United Kingdom

Abstract

Simulating the built environment for a globally distributed and diverse species e.g. to cope with climate change, has particular challenges. These are explored here using honey bees (*Apis Mellifera L*), a vital pollinator of food crops worldwide, consisting of 24 subspecies that maintain close temperature and humidity control in a self-constructed or partly human constructed built environment. Honey bee thermofluid characteristics and their requirements of the structure are largely unknown.

To address this an open source i.e. FreeCAD (Riegel and Mayer, 2019) and OpenFOAM (Jasak, Jemcov and Tukovic, 2007), computational fluid dynamics (CFD) conjugate heat model was developed.

Results from the model demonstrate the power of CFD in investigating the interactions with their built environment of another species by showing significant variation in convection flow with different honey bee sub-species in differing distributions within the nest.

Key Innovations

- Conjugate heat model of honey bee built environment including external and internal structures and occupants.
- Does not assume all honey bees are those from a single European sub species.
- Enables the simulation of sub-species differences as well as hive design and climatic impacts

Practical Implications

- This model enables refinement of the human contribution to hive design, to take into account subspecies and climate differences
- It enables determination of evolutionary factors that have changed honey bee physical characteristics and behaviours. This is important for enabling the continuing efficiency and survival of this pollinator in the face of climate change.

Introduction

Built environment simulation is almost completely focused on the relatively homogenous species *Homo sapiens*. However more diverse social species build structures that they inhabit.

The honey bee, a commercially important pollinator, has evolved several (circa 24) subspecies suited to diverse environments from tropical forests and semi-desert to temperate lands that have 233K winters. These subspecies vary in body diameter and body hair length (Ruttner, 1988) showing an increase of both in colder climates. Behaviours have evolved for selecting and manipulating their nest thermofluid environment including: nest cavity selection (usually a tree hollow) for thermal performance (e.g. volume, entrance size, entrance location); close temperature regulation in brood area via endothermy and advection; evaporation of large volumes of liquid (nectar to honey 200+kg per year) and the resulting water vapour transport (Mitchell, 2019); and clustering to reduce heat losses. Their construction of comb in the cavity reduces the large void of the nest cavity into a series of vertical narrow slots approximately 10mm wide with total free volume of only 30% of the original (Mitchell, 2022), the cell of the comb opening on to the slots with their long axis close to horizontal. In addition the honey bees coat the inside of the nest with a vapour retardant barrier made from plant resins propolis. They use the same material to close redundant openings in the cavity. They use this built environment to achieve both the temperature and humidity management for brood rearing i.e. 307K+/- 0.5, 80% RH and the low humidity (50%RH) required for the desiccation of low sugar concentration (20% to 40%) nectar in to high sugar concentration honey (82%+). The honey bees achieve this by self-organised zoned air conditioning via: sensitive temperature and humidity sensing on their antennae; heating using thorax muscles; ventilation through wing movements; and humidification by distributing water and dilute nectar throughout the nest. Further, the honey bees position themselves as obstructions to convective air currents as seen when they cluster in winter or when outside the nest (Heinrich, 1981).

Previous CFD research into honey bees inside their nest has not taken into account the global diversity in subspecies or climate, thermal properties of the hive walls or variation in honey bee distribution around the hive (Sudarsan *et al.*, 2012) . Similarly CFD research into other nest constructing species (*Macrotermes Michaelseni*, (Abou-Houly, 2010) *Polybia scutellaris*, (Hozumi *et al.*, 2011),) have only concentrated on single subspecies and climate and not taken account of the effect of the occupants.

The biological implications of this research for this species have been discussed in detail elsewhere

(Mitchell, 2022), while this paper will concentrate on the CFD modelling and verification.

Modelling an occupied structure necessitates not only knowledge of the environmental factor and the structure but also the key parameters of the inhabitants. Previous CFD research looked only at a single size of honey bee while treating it as a porous medium consisting of cylinders with a limited range of porosities located near the brood area. In order to address the global diversity in honey bees it was necessary in this research to include the full range of honey bee sizes and likely porosities.

Obtaining such information is challenging as often biological research has differing goals to building simulation and so in this case the dimensions have to be inferred indirectly from sizes of the cells in which the insects pupate. This is further complicated by subspecies having varying hair length which will change their effective dimensions (Ruttner, 1988), and human manipulation of body size by changing the cell size they use. The different subspecies have differing nest volumes and colony numbers in addition to body size. However from current research, it is possible to derive a range of honey bee diameters, lengths and number densities that cover the all of honey bee subspecies, see Table 1.

Table 1 Subspecies cell sizes, colony populations and volumes(Schneider and Blyther, 1988; Saucy, 2014; Mulisa et al., 2018)

Parameter	**Tropical**	**Temperate**
Nest Volume m^3 10^{-3}	17	45
Population 10^3	6.4	18.8
Cell diameter m 10^{-3}	2.5–4.3	4.4-5.5
Cell length m 10^{-3}	9.5-11.4	11-12
Distributed bee number density in inter-comb volume m^{-3} 10^6	1.25	1.39

Thus for given length and diameter and number density one can determine a porosity, equation 5, and hence an effective diameter in equation 4 (Li and Ma, 2011), which in turn can determine the coefficients that give the relationship between pressure differential per unit length and air velocity in equations 1,2, and 3 (Ergun and Orning, 1949).

$$\nabla P = -\alpha \vec{U} - \beta |\vec{U}| \vec{U} \quad (1)$$

$$\alpha = \mu 150 \frac{(1-\varphi)^2}{\overline{d}^2 \varphi^3} \quad (2)$$

$$\beta = \frac{\rho}{2} \frac{3.5(1-\varphi)}{\overline{d}\varphi^3} \quad (3)$$

$$\overline{d} = \frac{\pi^{\frac{1}{3}} (6V_P)^{\frac{5}{3}}}{A_P^2} \quad (4)$$

$$\varphi = 1 - \rho_B V_{Bee} \quad (5)$$

Most modern designs of man-made honey bee hive follow a pattern of stacked thin walled (~ 19mm) open top and bottom wooden box sections (~470 × 470 × 300 mm). On the top of the box sections is a thin plywood cover surmounted by a more substantial roof.

These sections sit on stand via a low floor section (~19 mm high) incorporating an entrance (10 x100mm) and a mesh covered opening beneath. So the same approach of modelling as porosity can be used to incorporate that feature in equations 6 and 7 (Idelchik, 2006)

$$\alpha = \mu \frac{11\varphi}{d_{orifice} L} \quad (6)$$

$$\beta = \frac{\rho}{2} \frac{1}{L} \left(1.3(1-\varphi) + \left(\frac{1}{\varphi} - 1 \right)^2 \right) \quad (7)$$

The small scale and complexity of internal features and passages (<5mm) combined with the much larger enclosure (~0.5m) created a challenge to simulate efficiently and comprehensively.

Simulation Methods

The world-wide adoption of similar pattern hives enabled the use of a common model for the enclosure (British National hive (Cushman, 2011)) as depicted in partial cross section in Figure 1. The CAD model was produced using FreeCAD with all of the construction parameters stored in MySQL.

The hive geometry provided particular challenges for meshing given a total volume of the simulation of 2 m^3 with the need to provide sufficient cells for solids and fluid details as small as 4mm. This was achieved using the OpenFOAM adaptive meshing tool snappyHexMesh layering feature as can be seen in Figure 2.

This enabled a high quality mesh with a minimum 4 cells in any dimension for any feature. It was tested for sensitivity by comparing results at 3.2 5.4 and 9.2 million cells. e.g Figure 3. They agreed closely with each other (<0.5%)

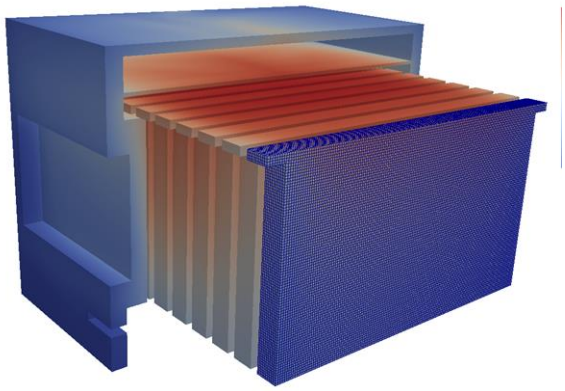

Figure 1 Cutaway of CFD model shows combs, cover board and roof

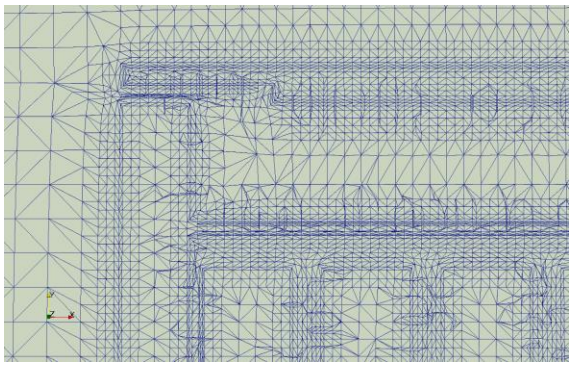

Figure 2 Meshing detail 3.2 million cells

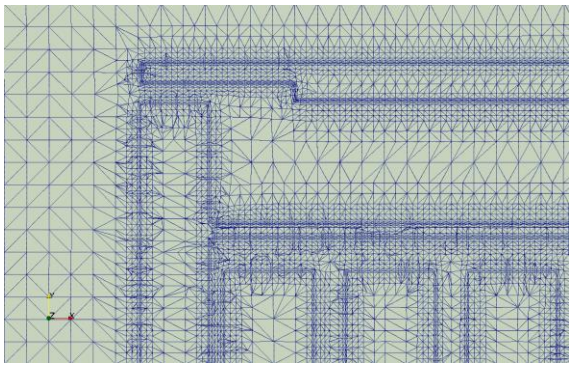

Figure 3 Meshing detail 9.2 million cells

The hive modelled was of 35 litres total capacity empty with 12 combs with centrally located constant temperature (307K) iso-thermal brood areas 214 × 100 mm in 6 of these combs. Two states of honey bee distribution were modelled, *"brood covering"* and "*distributed*". In the *distributed* state the bees were assumed to be at uniform number density in all of the free space within 10mm of the combs. In the *brood covering* state the honey bees were assumed to be solely located in 340 by 140 by 10mm volumes adjacent to each brood area. The only heat generation being the brood areas. Radiation was ignored. A standard compressible flow, steady state conjugate multi-region heat transfer solver, CHTmultiRegionSimpleFoam was used. As laminar flow was likely, but uncertain, a kω-SST turbulence model was selected with inlet turbulent energy, turbulent dissipation rate and specific turbulent dissipation rate set to fixed values according to the literature(CFD Online, 2014b). The OpenFOAM feature fvOptions was used to generate the porosity zone simulating the honey bees and the floor wire mesh and the constant temperature zone simulating the brood within the comb. An enthalpy modifying field was used to give the varying conductivity zones within the comb regions to simulate the wooden frame (0.12 Wm^{-1}) the empty comb (0.023Wm^{-1}) and the brood (0.6Wm^{-1}) using values from the literature (Humphrey and Dykes, 2008). The hive cover board and roof were modelled as separate regions with a conductivity of 0.12Wm^{-1} . Condensation, evaporation and conductivity of the honey bees were not considered.

A separate CFD run was conducted for each combination of:

- Honey bee effective diameter, (2.5,4.0,5.5mm)
- Honey bee porosity 0.09 to 1.0
- Brood covering or distributed states,
- Ambient temperature. (263,273,283,293K)

The iteration steps were continued until the temperatures within the model reached equilibrium, typically after 3500 iterations. For post-processing, the heat flux from the frames into the surrounding air was computed from each of the runs using the wallHeatFlux ((Venkatesh, 2016)) post-processing function similarly for the y^+ (CFD Online, 2014a) turbulence metric. In addition Paraview (Ayachit, 2015), was used to derive visualisations of temperature and air flow. The results along with the key parameters were loaded into an open source SQL database (Ayachit, 2015) and then plotted using MATlab (MATLAB, 2018).

Validation methods

Validation against a hive occupied with a live honey bee colony was impractical so an in-vitro analogue for the contents of the hive was substituted so that validation of the model of a hive with brood heating but without honey bees could be accomplished. A hive with comb frames were sourced from a commercial supplier and the combs made from foam with a similar thermal conductance (Humphrey and Dykes, 2008). The isothermal brood areas in the 6 combs were constructed from a sandwich of 2 aluminium plates and a serpentine resistance wire to which was attached a digital thermal sensor (MicroChip, 2005) see Figure 4.

Figure 4 Brood frame analogue

There is also a problem trying to map directly the CFD model results to experimental results, as the CFD model does not include the radiation from the hive surface and radiation passed through the floor mesh and absorbed re-radiated by the floor mesh,

The radiation is surprisingly significant in this problem owing to the large surface areas (~0.8 m^2) involved for such a relatively small heat input (~10W), where a 1K surface temperature above ambient gives rise to a net radiation of 4.5W (equation 21). This radiation is large enough to be used to locate the position and size of the honey bee cluster, in thin walled wooden hives, in winter, using infrared thermography (Figure 5) (Shaw et al., 2011).

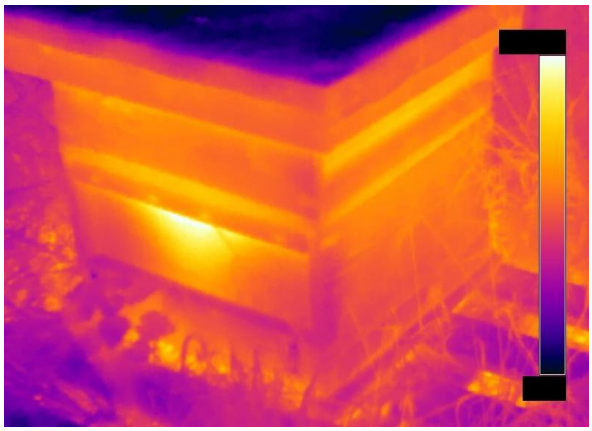

Figure 5 Infra-red thermograph of a hive (AIRSS Ltd)

Thus the validation experiment and analysis were fashioned to overcome this issue by considering the surface temperatures in both the validation analysis and the experiment.

For the experiment, the heater wattage was set to give heated plate/brood temperatures in the range of 14 to 20K above ambient after a period of 48 hours. At equilibrium, temperatures of the top surface of hive and the mesh underneath were measured for a period of 24 hours using 26 digital surface temperature sensors. The distribution of the individual sensors within a patch utilised an Optimised Latin Hypercube sampling method (Morris and Mitchell, 1995). By the use of symmetry, the cross-calibrated sensors were arranged in patches to achieve the same effect as 78 sensors distributed across the entire surface (Figure 6).

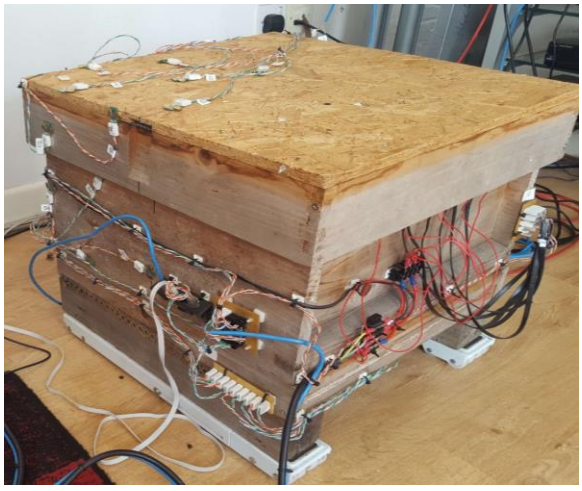

Figure 6 Hive with networked contact thermometers

For analysis , the approach taken is to compare the CFD (*cfd*) model (Figure 7a) of a hive with brood heating but without honey bees and the experiment (*exp*) (Figure 7b) via two lumped thermal models, radiating (*lr*) (Figure 7d), and non-radiating (*lnr*) (Figure 7c), where the conductive and convective resistances are more easily analysed.

We set the following: identical conductive/convective resistances and input energies between CFD and lumped non-radiative (*lnr*), and between experimental and lumped radiative (*lr*) equations 7,8, and 13; The ambient and brood temperature are identical in all models equation 9 and 10*;* The *lr* mesh temperature equals the average experimental mesh temperature and thus the downward radiative energies equation 12.

$$R_{SA(lnr)} = R_{SA(cfd)}, \quad R_{SA(lr)} = R_{SA(exp)} \tag{6}$$

$$R_{CS(lnr)} = R_{CS(cfd)}, \quad R_{CS(lr)} = R_{CS(exp)} \tag{7}$$

$$T_{B(cfd)} = T_{B(lnr)} = T_{B(lr)} = T_{B(exp)} \tag{8}$$

$$T_{A(cfd)} = T_{A(lnr)} = T_{A(lr)} = T_{A(exp)} \tag{9}$$

$$T_{M(lr)} = T_{M(exp)} \tag{10}$$

$$\dot{q}_{CA(lr)} = \dot{q}_{CA(exp)}, \dot{q}_{CM(lr)} = \dot{q}_{CM(exp)} \tag{11}$$

$$\dot{q}_{E(lnr)} = \dot{q}_{E(cfd)} \quad \dot{q}_{E(lr)} = \dot{q}_{E(exp)} \tag{12}$$

From energy balance then if equation 14 is true then equations 15 and 16 are also true.

$$\dot{q}_{SAR(exp)} = \dot{q}_{SAR(lr)} \tag{13}$$

$$R_{CS(cfd)} = R_{CS(lnr)} = R_{CS(lr)} = R_{CS(exp)} \tag{14}$$

$$R_{SA(cfd)} = R_{SA(lnr)} = R_{SA(lr)} = R_{SA(exp)} \tag{15}$$

Therefore, the goal is changed to one where we prove that the surface to ambient convective thermal resistance (R_{SA}) and the hive comb to surface convective thermal resistance (R_{CS}) are similar, in all four models for conduction convection, at the temperatures and energy fluxes involved

We can analyse the lumped models via the thermal circuits in figures Figure 8 and Figure 9.

The *lnr* convective resistances in equations 16 and 17 can derived

$$R_{CS(lnr)} = \frac{T_{B(cfd)} - T_{S(lnr)}}{\dot{q}_{E(cfd)}} \tag{16}$$

$$R_{SA(lnr)} = \frac{T_{S(lnr)} - T_{A(cfd)}}{\dot{q}_{E(cfd)}} \tag{17}$$

If the downward radiation is considered to be 7 slots at brood temperature using view factors we determine trhe downward radiations in equations 18 and 19

$$\dot{q}_{CM(exp)} = \sigma(1-\varphi)\Sigma A_i f_i \left(T^4_{B(exp)} - T^4_{M(exp)}\right) \tag{18}$$

$$\dot{q}_{CA(exp)} = \epsilon_M \sigma \varphi \Sigma A_i f_i \left(T^4_{B(exp)} - T^4_{A(exp)}\right) \tag{19}$$

the *lr* surface temperature is given by equation 20

$$T_{S(lr)} = T_{B(lr)} - \left(\dot{q}_{E(lr)} - \dot{q}_{CA(lr)} - \dot{q}_{CM(lr)}\right) R_{CS(lr)} \tag{20}$$

The lr surface radiative and convective energy fluxes equations 21 and 22

$$\dot{q}_{SAR(lr)} = \sigma \epsilon_S A_S \left(T^4_{S(lr)} - T^4_{A(exp)}\right) \tag{21}$$

$$\dot{q}_{SA(lr)} = \frac{T_{S(lr)} - T_{A(exp)}}{R_{S(lr)}} \tag{22}$$

The energy balance is expressed as equation 23

$$\dot{q}_{E(exp)} - \dot{q}_{CM(exp)} - \dot{q}_{CA(exp)} - \dot{q}_{SA(lr)} - \dot{q}_{SAR(lr)} = 0 \tag{23}$$

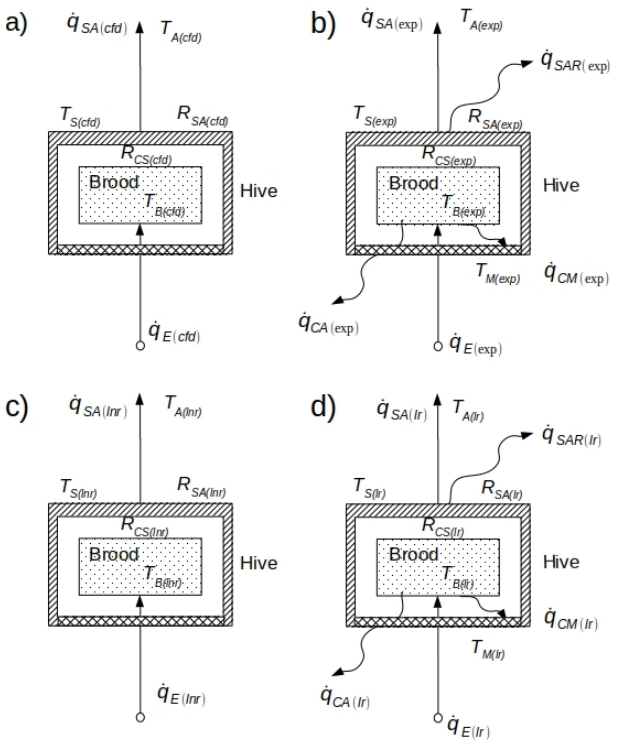

Figure 7 schematic of thermal models a) CFD, b) experiment(exp), c)lumped non radiative(lnr), d) lumped radiative(lr)

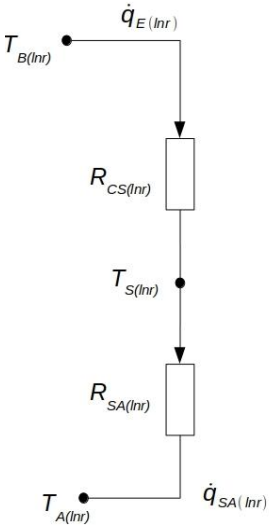

Figure 8 Lumped thermal models Non-radiative (lnr)

If the convective resistances are equal then equation 23 can then be solved numerically to determine $T_{S(lr)}$.With solutions of $T_{S(lr)}$ known, the values of $\dot{q}_{SAR(lr)}$, can be determined for values of $\dot{q}_{E(exp)}$.$\dot{q}_{E(lr)}$ and $\dot{q}_{CA(exp)}$.

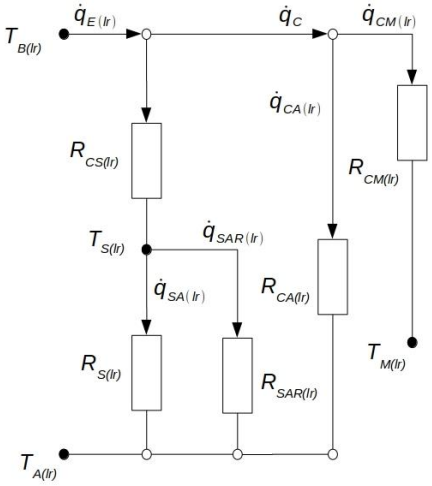

Figure 9 Lumped thermal model Radiative (lr)

Model Results

Given the complexity of the problem it is useful to understand how key parameters interact before interpreting the CFD results. The low velocity dominant coefficient α from equations 1 and 2 is plotted versus actual honey bee diameter at values of constant number density and actual honey bee length in Figure 10.

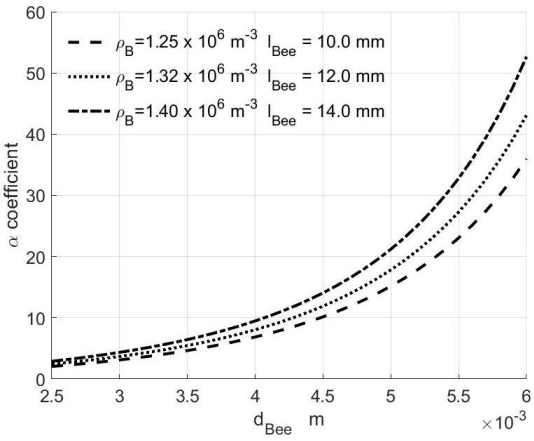

Figure 10 Flow resistance coefficient α versus actual bee diameters d_{Bee} at constant bee number densities ρ_B

The plot of hive thermal resistance vs honey bee number density in the *distributed* state shown in Figure 11. Similarly for the *brood covering* state, hive thermal resistance versus porosity in Figure 12. Both plots are at constant ambient temperature 293K and effective diameter sizes.

Validation Results

Three experimental runs at approximately 10, 15 and 20W yielded the brood and ambient temperatures as shown in Table 2. Matching CFD runs were completed at those temperatures. The values of $\dot{q}_{E(cfd)}$ were extracted from the CFD runs and the values of $\dot{q}_{E(exp)}$, $\dot{q}_{C(exp)}$ and $\dot{q}_{SAR(exp)}$ extracted from the experiment.

$\dot{q}_{SAR(lr)}$ was determined as described above and tabulated in Table 2.

To check the sensitivity of this approach for a given $\dot{q}_{E(exp)}$ values of $\dot{q}_{SAR(lr)}$ were plotted against values of $\dot{q}_{E(cfd)}$ and $\dot{q}_{C(exp)}$. The plot for $\dot{q}_{E(exp)} = 20W$ is shown in Figure 13.

Table 2 Physical Experiment Parameters and results for 10W 15W and 20W $\dot{q}_{E(exp)}$

	Run Values		
parameter	**10W**	**15W**	**20W**
$T_{B(exp)}$ K	308.71	314.66	319.69
$T_{A(exp)}$ K	293.96	294.52	294.44
$\dot{q}_{E(exp)}$ W	10.19 ± 1%	15.08 ± 1%	20.09 ± 1%
$\dot{q}_{SAR(exp)}$ W	6.08 ± 15%	8.61 ± 11%	10.51 ± 8%
$\dot{q}_{SAR(lr)}$ W	5.32	7.85	10.19
$\dot{q}_{E(cfd)}$ W	6.40	9.62	13.10
$\dot{q}_{C(exp)}$ W	2.45 ± 5%	3.44 ± 4%	4.44 ± 3%
Validation error	12%	9%	3%

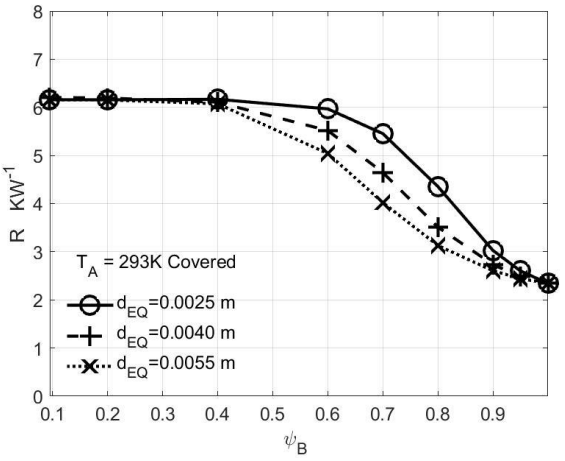

Figure 11 Brood covering hive thermal resistance vs porosity for constant effective diameters T_A = 293K

Discussion

Almost all building simulation is for human occupants from a single extant subspecies, so it is important to test our inbuilt assumptions. Honey bees have been used to test anthropogenic assumptions in others fields and have proved useful (Dyer, Neumeyer and Chittka, 2005). This research confirms this. The most obvious difference is size and their lack of confinement to floors, however, if we use a dimensionless occupancy i.e. occupants per occupant volume (Nr density* Table 3) other differences emerge. Thus we can see honey bees have a dimensionless occupancy of 1 to 2 orders of magnitude higher than humans and have an order of magnitude variation between subspecies.

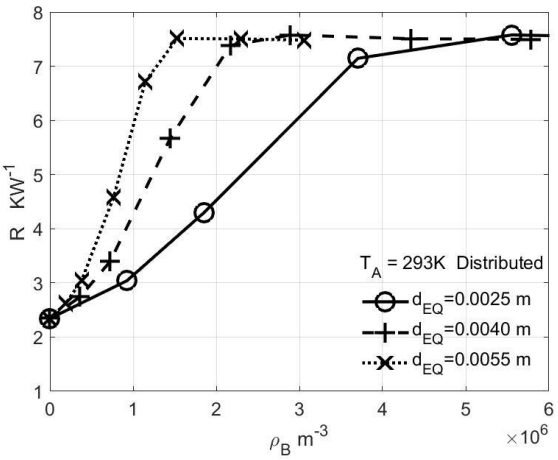

Figure 12 Distributed hive thermal resistance vs colony number density for effective diameters at constant ambient temperature 293K. The rightmost termination of the lines for distributed indicates the geometric packing limit with the exception of 2.5mm diameter

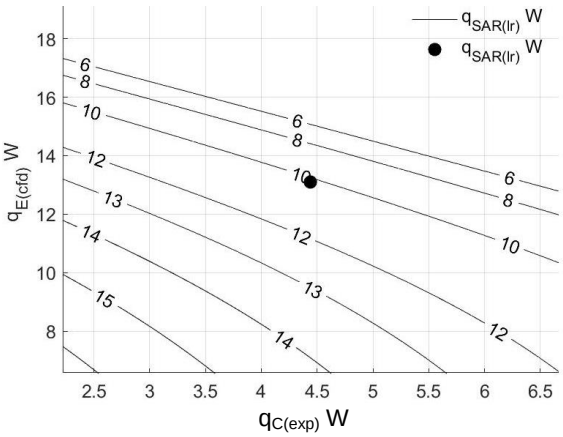

Figure 13 Plot of lumped hive surface radiation flux $\dot{q}_{SAR(lr)}$ for CFD input power $\dot{q}_{E(cfd)}$ and mesh radiation flux $\dot{q}_{M(exp)}$where $\dot{q}_{E(exp)}$ = 20W(c) with the experimental $\dot{q}_{SAR(lr)}$ point value

The CFD simulation of the built environment likewise shows striking differences between the subspecies as can be seen in Figure 12 where although the distributed number density for both sub species is similar (1.3 to 1.4) the effect on thermal resistance is dramatic, giving 7 to 3.5 a factor of two. This marked difference is based on the flow resistance physics shown in Figure 10. Here we can clearly see for constant number density the diffusive coefficient, α, increases as the 3rd power of the honey bee diameter. This means that temperate honey bees are close to stopping convective heat transfer within their hive, yet the tropical subspecies will have considerable convective heat transfer. This shows that temperate honey bees need to create bee-less spaces in order to efficiently move air around their hive e.g. for removing water vapour from nectar desiccation. This behaviour has been observed in honey bee clusters (Heinrich, 1981) .

The validation has shown radiation to be significant. Given the low temperatures involved this may be surprising to some. The validation technique used has shown that this simulated convection model has an accuracy within or close to the scope of the experimental error Table 2.

Table 3 Dimensionless comparison of human and honey bee occupancy (Department for Communities and Local Government, 2015)

Parameter	Humans	Temperate bee	Tropical bee
length m	1.7	0.014	0.011
diameter m	0.6	0.0055	0.0025
occupant m^3	4.8E-01	3.3E-07	5.4E-08
dwelling m^3	300	0.014	0.0051
occupants	8	1.8E+04	6.4E+03
Nr density m^{-3}	2.7E-02	1.4E+06	1.3E+06
dwelling volume*	6.3E+02	4.1E+04	9.5E+04
Nr density*	1.3E-02	4.7E-01	6.8E-02

Conclusion

This research shows that when simulating unfamiliar constructions and occupants it is necessary to challenge assumptions. Here we have demonstrated that unlike anthropocentric experience, it possible for relatively small subspecies differences to have marked effects on the thermal performance of the built environment that can be as least significant as the change in the thermal performance of the individual animal. In this case the changing building performance by a factor of 2. Further it has shown that while radiation can be a surprisingly significant factor, it does not prevent significant simulation results being validated.

. *Table 4 Nomenclature*

Symbol*	Units	Description
∇P	N m^{-3}	Pressure differential per unit length
$\vec{U}$	ms^{-1}	Velocity
β	kgm^{-4}	2^{nd} order velocity coefficient (impact)
α	$Nm^{-4}s$	1^{st} order velocity coefficient (viscous)
μ	$Nm^{-2}s$	Dynamic viscosity
φ	-	Porosity
ρ	kgm^{-3}	Density
$\bar{d}$	m	Generic effective diameter
V_P	m^3	Volume of particle
A_P	m^2	Surface area of particle
$\overline{d}$	m	Effective particle diameter
d_{orifac}	m	Effective diameter of mesh opening
L	m	Depth of mesh in simulation
ρ_B	m^{-3}	Honey bees per unit volume
V_{Bee}	m^3	Average volume of individual bee
A_S	m^2	Area of hive surface less the area of underfloor mesh
A_i	m^2	Area of inter-comb gap element (i) on Hive internal top surface
f_i	-	View factor of inter-comb gap element (i) on Hive internal top surface
$R_{CS(j)}$	$W^{-1}K$	Brood comb to hive surface lumped thermal resistance*
$R_{SA(j)}$	$W^{-1}K$	Hive external surface to ambient convective/conductive thermal resistance*
$R_{SAR(j)}$	$W^{-1}K$	Hive external surface to ambient radiative resistance*
$R_{CM(j)}$	$W^{-1}K$	Hive internal top surface mesh pass through radiative resistance*
$R_{CA(j)}$	$W^{-1}K$	Hive internal top surface mesh absorptive radiative resistance*
$\dot{q}_{E(j)}$	W	Brood comb heat flux*
$\dot{q}_{C(j)}$	W	Sum of radiated heat flux from brood comb downwards*
$\dot{q}_{CA(j)}$	W	Estimated downwards radiated heat flux brood comb to wire mesh absorbed*
$\dot{q}_{CM(j)}$	W	Downwards radiated heat flux brood comb to ambient*
$\dot{q}_{SA(j)}$	W	Convective/conductive heat flux hive top surface to ambient*
$\dot{q}_{SAR(j)}$	W	Radiated heat flux hive top surface to ambient*
$T_{S(j)}$	K	Hive surface temperature*
$T_{A(j)}$	K	Ambient temperature*
$T_{B(j)}$	K	Brood temperature*
$T_{M(j)}$	K	Temperature of wire mesh - physical experiment*
σ	$Wm^{-2}K^{-4}$	Stephan-Boltzmann constant 5.8 x 10^{-8}
ε_m	-	Emissivity of hive floor metal mesh 0.9
ε_S	-	Emissivity of hive external surface 0.9
φ	-	Porosity of hive floor mesh

Note :* j is one of *cfd, exp, lr, and lnr* models used in validation.

Acknowledgements

The University of Leeds high performance computing (HPC) facility, ARC, was used as well as the authors own HPC facility.

Data Availaibility

Data available on request from the authors.

References

Abou-Houly, H. E. (2010) *Investigation of flow through and around the Macrotermes michaelseni termite mound skin*. Loughborough University. Available at: https://dspace.lboro.ac.uk/2134/8466.

Ayachit, U. (2015) *The ParaView Guide: A Parallel Visualization Application*. Kitware, Incorporated.

CFD Online (2014a) *Dimensionless wall distance (y plus), Wiki*. Available at: https://www.cfd-online.com/Wiki/Dimensionless_wall_distance_(y_plus) (Accessed: 10 March 2021).

CFD Online (2014b) *Turbulence free-stream boundary conditions*. Available at: ttps://www.cfd-online.com/Wiki/Turbulence_free-stream_boundary_conditions (Accessed: 10 March 2021).

Cushman, D. (2011) *Drawings of Hives and Hive Parts, Dave Cushman's Beekeeping and Bee Breeding Website*. Available at: http://www.dave-cushman.net/bee/natdrawings.html.

Department for Communities and Local Government (2015) 'Statutory guidance: Technical housing standards – nationally described space standard', 2016(30th June). Available at: https://www.gov.uk/government/publications/technical-housing-standards-nationally-described-space-standard.

Dyer, A. G., Neumeyer, C. and Chittka, L. (2005) 'Honeybee (Apis mellifera) vision can discriminate between and recognise images of human faces.', *The Journal of experimental biology*, 208(Pt 24), pp. 4709–4714. doi: 10.1242/jeb.01929.

Ergun, S. and Orning, A. A. (1949) 'Fluid Flow through Randomly Packed Columns and Fluidized Beds', *Industrial & Engineering Chemistry*, 41(6), pp. 1179–1184. doi: 10.1021/ie50474a011.

Heinrich, B. (1981) *The Mechanisms and Energetics of Honeybee Swarm Temperature Regulation*, *J. Exp. Biol.* doi: 10.1126/science.212.4494.565.

Hozumi, S. *et al.* (2011) 'Thermal characteristics of polybia scutellaris nests (Hymenoptera: Vespidae) using computational fluid dynamics: A possible adaptation to tropical climates', *Sociobiology*, 57(1), pp. 123–141.

Humphrey, J. A. C. and Dykes, E. S. (2008) 'Thermal energy conduction in a honey bee comb due to cell-heating bees', *Journal of Theoretical Biology*, 250(1), pp. 194–208. doi: 10.1016/j.jtbi.2007.09.026.

Idelchik, I. E. (2006) 'Handbook of hydraulic resistance (3rd edition)', *Washington*. doi: AEC-tr- 6630.

Jasak, H., Jemcov, A. and Tukovic, Z. (2007) 'OpenFOAM : A C ++ Library for Complex Physics Simulations', *International Workshop on Coupled Methods in Numerical Dynamics*, m, pp. 1–20.

Li, L. and Ma, W. (2011) 'Experimental Study on the Effective Particle Diameter of a Packed Bed with Non-Spherical Particles', *Transport in Porous Media*, 89(1), pp. 35–48. doi: 10.1007/s11242-011-9757-2.

MATLAB (2018) *9.4.0.813654 (R2018a)*. Natick, Massachusetts: The MathWorks Inc. Available at: https://uk.mathworks.com/help/matlab/.

MicroChip (2005) '2-Wire Serial Temperature Sensor TCN75A', pp. 1–30.

Mitchell, D. (2019) 'Nectar, humidity, honey bees (Apis mellifera) and varroa in summer: A theoretical thermofluid analysis of the fate of water vapour from honey ripening and its implications on the control of Varroa destructor', *Journal of the Royal Society Interface*, 16(156). doi: 10.1098/rsif.2019.0048.

Mitchell, D. M. (2022) 'Honey bee (Apis mellifera) size determines colony heat transfer when brood covering or distributed', *International Journal of Biometeorology*, pp. 1653–1663. doi: 10.1007/s00484-022-02308-z.

Morris, M. D. and Mitchell, T. J. (1995) 'Exploratory designs for computational experiments', *Journal of Statistical Planning and Inference*, 43(3), pp. 381–402. doi: 10.1016/0378-3758(94)00035-T.

Mulisa, F. *et al.* (2018) 'Determination of bee spacing and comb cell dimensions for Apis mellifera Scutellata honeybee race in western Ethiopia', *International Journal of Livestock Production*, 9(8), pp. 206–210. doi: 10.5897/ijlp2018.0484.

Riegel, J. and Mayer, W. (2019) 'FreeCAD (Version 0.18)'.

Ruttner, F. (1988) *Biogeography and Taxonomy of Honeybees*. doi: 10.1093/ae/36.1.58.

Saucy, F. (2014) 'On the natural cell size of European honey bees: a "fatal error" or distortion of historical data?', *Journal of Apicultural Research*, 53(3), pp. 327–336. doi: 10.3896/IBRA.1.53.3.01.

Schneider, S. and Blyther, R. (1988) 'The habitat and nesting biology of the African honey bee Apis mellifera scutellata in the Okavango River Delta, Botswana, Africa', *Insectes Sociaux*, 35(2), pp. 167–181. doi: 10.1007/BF02223930.

Sudarsan, R. *et al.* (2012) 'Flow currents and ventilation in Langstroth beehives due to brood thermoregulation efforts of honeybees', *Journal of Theoretical Biology*, 295(November), pp. 168–193. doi: 10.1016/j.jtbi.2011.11.007.

Venkatesh, V. (2016) 'CFD with OpenSource software Tutorial of convective heat transfer in a vertical slot', *Proceedings of CFD with OpenSource Software*. Available at: http://www.tfd.chalmers.se/~hani/kurser/OS_CFD_2016/VarunVenkatesh/Varun_report.pdf.